

Tuning surface texture of electrospun polycaprolactone fibers: Effects of solvent systems and relative humidity

Murat Şimşek^{1,a)}

¹Department of Biomedical Engineering, Inonu University, Malatya 44280, Turkey

^{a)}Address all correspondence to this author. e-mail: murat.simsek@inonu.edu.tr

Received: 2 September 2019; accepted: 7 January 2020

In this study, the surface morphology of electrospun polycaprolactone (PCL) fibers was investigated. PCL was dissolved in various solvent/nonsolvent systems (acetone/dimethylformamide (DMF), tetrahydrofuran (THF)/DMF, dichloromethane (DCM)/DMF, chloroform (CF)/DMF, acetone/dimethyl sulfoxide (DMSO), THF/DMSO, DCM/DMSO, CF/DMSO) at a fixed ratio of 80/20 v/v. PCL solutions from these solvent systems were electrospun under varying high relative humidity (60–90%), and also room humidity. Characterization of fibers was evaluated by a scanning electron microscope, an atomic force microscope, water contact angle measurements, the Brunauer–Emmett–Teller method, and a strain–stress test. Results revealed that the surface texture of individual fibers changed with the presence of different types of pores and surface roughness depending on both humidity and solvent/nonsolvent properties. Miscibility with water was another factor to be taken into account for understanding mechanisms that contributed to the formation of surface defects. Fibrous materials having such a surface architecture, especially the porous ones, are potential candidates for various applications such as tissue engineering, drug delivery, catalysis, and filtration.

Introduction

The electrospinning technology is often used to obtain interconnected nano/micro fiber mats for many applications ranging from medicine to engineering [1, 2, 3, 4]. Electrospun fibers have many advantages such as exceptional surface area to volume ratio, controllable pore structure, high porosity, flexible surface properties, high functionality, and superior mechanical properties. It is possible to obtain nonwoven fibers at various morphologies with this technique.

Polycaprolactone (PCL) is a family member of biodegradable aliphatic polyesters which has important use as a bio-material. As a commercial material, the main attractions of PCL are (i) its approval by the food and drug administration (FDA) for use in humans, (ii) its biodegradability, (iii) its compatibility with a wide range of other polymers, (iv) its good processability, (v) its high thermal stability, and (vi) its relatively low cost [5].

In recent years, great attention has been focused on the synthesis of porous fibers through different phase separation processes for applications in the energy, environmental, and biomedical industries [6, 7, 8, 9, 10]. The remarkable advantage

of porous fibers over those with a smooth surface is the higher specific surface area to favor cellular behavior in tissue engineering applications [10, 11, 12]. Surface porosity also facilitates the transition of air and nutrients into fibrous mats for the survival of cells inside the matrix. Furthermore, pores can absorb the stress applied on the fiber surface, owing to an increase in the toughness of fibers [13].

Several attempts have been made to change the surface topography of electrospun fibers for various applications by using humidity [14, 15], phase separation processes [16], additives [17], and bath collector [18]. By considering the advantage of the single-step process, the surface texture of electrospun fibers can be changed by using high relative humidity (RH) and/or solvent mixtures. In a humid atmosphere, water vapor can be condensed on the surface leaving an imprint. Subsequently, the evaporation of water molecules from the surface leads to the formation of circular pores in the form of nano- to micron-sized patterned array of defects, which is referred to as breath figures [19]. These pores appear only at the surface and not deep inside the fiber. As an alternative, the surface topography of fibers can be tuned by

vapor-induced phase separation (VIPS) which is triggered by the absorption of water vapor in a humid atmosphere onto fiber surfaces [16]. Although several studies have been carried out recently [7, 16, 20], there are very limited studies that investigate the effect of RH on the morphology of electrospun PCL fibers. In a study, PCL was electrospun at a range of relative humidities (5–75%). A chloroform (CF)/DMF solvent system at a ratio of 80:20 v/v was used to evaluate the effect of RH on electrospun PCL fiber morphology [21]. In another study, PCL solutions were prepared by using pure solvents of dichloromethane (DCM), CF, and solvent mixtures of CF:methanol with a volume ratio of 18:2 and CF:DMSO with volume ratios of 19:1, 18:2, and 16:4, respectively. All solutions were processed into fibers at three different conditions, 12, 35, and 55% RH, respectively [22].

Another mechanism that causes phase separation is non-solvent-induced phase separation (NIPS). In this technique, a solvent is mixed with an appropriate ratio by a nonsolvent liquid which has a higher boiling point than that of the solvent used and does not dissolve the polymer used [7, 23, 24]. The initiation of the phase separation process can be induced by the thermodynamic instability of the solution in the presence of a nonsolvent. Georgiadou et al. [7] investigated the effect of different solvent systems on the surface morphology and the size of electrospun PCL fibers through the NIPS mechanism. Their design involved the use of solvent mixtures composed of good and poor solvents for PCL in various ratios. Solvents chosen in their work were CF, DCM, tetrahydrofuran (THF) and formic acid, whereas DMSO was chosen as the nonsolvent. In another study, PCL was electrospun using different solvents (CF/diethyl ether, CF/ethyl acetate, CF/DCM, CF/DMSO, CF/DMF, and CF/ethanol) with the influence of different vapor pressures to investigate the morphology, diameter, and mechanical properties of the electrospun fibrous scaffolds [25]. The results showed that the vapor pressure of the solvents and/or mixture solvents played an important role in the morphology of the fibers.

Although the effect of humidity on the morphology of electrospun fibers was investigated in some studies, no systematic investigation was presented in the literature to reveal the relationship between solvent/nonsolvent systems and RH, and its effect on the surface morphology of electrospun PCL fibers. In the presented study, the effect of RH in the range of 60–90% on the morphology of the fibers was examined in the presence of different solvent/nonsolvent systems using acetone (ACT), THF, DCM, or CF as solvents, and DMF or DMSO as nonsolvents. The main purpose of the study was to examine different phase separation mechanisms that managed to alter the surface textures of PCL fibers.

Results and discussion

In the presented study, various solvent/nonsolvent systems were examined at given RH conditions to observe as-spun PCL

fiber morphologies. The reason behind the choice of solvent/nonsolvent systems is that each solvent or nonsolvent has different physical properties and characteristics (Table I); that is, all of the PCL solutions prepared had different properties. Thus, it would be possible to elucidate their effects on the surface morphology of electrospun PCL fibers. DMF and DMSO with a relatively higher boiling point and dielectric constant were selected as nonsolvents, whereas ACT, THF, DCM, and CF were chosen as solvents for PCL. All solvent/nonsolvent systems used for dissolving PCL are miscible. For experimental setup, various PCL solutions with a fixed solvent/nonsolvent ratio of 80/20 v/v were prepared, and the electrospinning of the solutions was performed at 60, 70, 80, and 90% RH conditions. The fibers were also produced at room humidity (26–28%) as a control. The electrospinning of PCL solutions was carried out at similar conditions presented in Table II for each solvent/nonsolvent system. However, it was necessary to adjust the applied voltage to achieve a stable jet for the samples from THF/DMSO and DCM/DMSO.

Table II also represents fiber diameters for as-spun PCL fibers. Although fiber diameters tended to increase with increasing RH in the case of ACT/DMF and ACT/DMSO solvent systems, the effect of each nonsolvent became ambiguous in terms of diameters. Similar results occurred in the fibers from THF-based solvents. However, fiber diameters decreased with increasing RH in the presence of DCM/DMF. When DMSO was chosen as the nonsolvent, a logical effect on the diameter relating to increasing RH could not be observed on the fibers. In the case of CF-based solutions, whereas fiber diameters tended to decrease in the presence of DMF, the opposite behavior occurred for DMSO. The results also revealed that the diameters were highly affected by RH and exhibited a wide range distribution depending on the type of solvent system. An interesting comparison can be done in terms of the fiber diameter–morphology relation under the same RH. At 60% RH, PCL fibers from DCM/DMSO-60 and CF/DMSO-60 had a porous morphology that was absent those from DCM/DMF-60 and CF/DMF-60. In this case, stretching forces on the porous or defected fibers could lead to more elongation in mechanically weaker fibers because of pores and/or defects in the fiber structure, and thus the fiber diameter decreased. A similar situation also occurred on the samples from DCM/DMF, DCM/DMSO, CF/DMF, and CF/DMSO at 90% RH. Electrospinning is a complex process, and it takes many factors into consideration to clarify the formation of fibers at different physical properties. To fully understand the relationship of fiber diameter–RH–solvent systems, electrospinning conditions (mainly applied voltage, flow rate, fiber collecting distance, and RH) and solvent system's properties such as conductivity, viscosity, and surface tension all should be taken into

TABLE I: Solvent characteristics used in the study.

Solvents	Boiling point (°C)	Miscibility with water	Solvent/nonsolvent for PCL	Dielectric constant at 20 °C	Vapor pressure at 20 °C (hPa)
ACT	56.1	Miscible	Solvent	21	233
THF	66	Miscible	Solvent	7.5	173
DCM	40	Immiscible	Solvent	9.1	470.9
CF	61.6	Immiscible	Solvent	4.8	211
DMF	153	Miscible	Non-solvent	38.3	3.77
DMSO	189	Miscible	Non-solvent	46.6	0.6
Water	100	...	Non-solvent	...	23.34

consideration step by step with an experimental study, which was not our aim in the presented study. In conclusion, the obtained results revealed that the combined effects of each solvent/nonsolvent system, their miscibility with water from the humid environment, and the electrospinning conditions gave rise to the fibers at different overall morphology and diameters.

Surface morphologies of the fibers were examined by a scanning electron microscope (SEM) analysis, and these results are presented in Figs. 1–4. Figures 1(a)–1(e) show the images of PCL fibers prepared with the ACT/DMF solvent system in the presence of different RH. Although overall morphologies of the fiber surfaces resembled each other, some samples exhibited grooved and pitted surface topography [Figs. 1(d) and 1(e)]. Nanosized indentations down to 100 nm also draw attention for ACT/DMF-70 [Fig. 1(c)]. The fiber surfaces exhibited minimal patterned topography in the presence of room humidity (rh) [Fig. 1(a)]. When compared with the ACT/DMF solvent system, the effect of RH on the surface morphology of PCL fibers was much more pronounced for the ACT/DMSO solvent system [Figs. 1(f)–1(j)]. The fiber surfaces were covered by crater-like shapes (breath figures), including a small amount of irregular pores at the nanometer size range (between 10- and 50-nm size ranges). Surface defects on the control samples also draw attention [Fig. 1(f)]. According to Figs. 2(a)–2(e), all of the THF/DMF-based surfaces had a similar morphology, where the fiber surfaces showed a smooth structure and very small-sized indentations with an increasing amount. However, the surface topography changed clearly in the presence of DMSO under all RH conditions [Figs. 2(f)–2(j)]. When compared with the control group with eroded texture [Fig. 2(f)], the fiber surfaces included both open and interconnected pores and also had breath figures in an irregular manner [Figs. 2(g) and 2(j)]. The altered topography was much more distinguished for THF/DMSO-70 [Fig. 2(h)] and THF/DMSO-90 [Fig. 2(i)] samples. As indicated in Figs. 3(b) and 3(c), the fibers from DCM/DMF-60 and DCM/DMF-70 exhibited wrinkly and grooved arranged texture. Pore formation was observed when RH increased to

TABLE II: Conditions for obtaining PCL fibers, their abbreviations, and diameters.

RH (%)	Sample abbreviation	Electrospinning conditions	Diameters (nm) ± SD	Diameters in the range (~nm)
60	ACT/DMF-60	17 kV, 2 mL/h, 23 cm	943 ± 402	400–2200
70	ACT/DMF-70	...	914 ± 378	440–2400
80	ACT/DMF-80	...	1050 ± 470	430–2700
90	ACT/DMF-90	...	1240 ± 877	410–3500
60	ACT/DMSO-60	17 kV, 2 mL/h, 23 cm	1000 ± 356	400–1900
70	ACT/DMSO-70	...	1670 ± 810	710–4600
80	ACT/DMSO-80	...	1260 ± 421	370–2900
90	ACT/DMSO-90	...	1270 ± 759	400–3000
60	THF/DMF-60	17 kV, 1 mL/h, 23 cm	861 ± 606	300–2600
70	THF/DMF-70	...	955 ± 400	390–2100
80	THF/DMF-80	...	838 ± 313	300–1700
90	THF/DMF-90	...	1100 ± 405	320–1900
60	THF/DMSO-60	15 kV, 1 mL/h, 23 cm	1005 ± 380	240–2100
70	THF/DMSO-70	...	1150 ± 533	260–3200
80	THF/DMSO-80	...	1388 ± 494	470–3200
90	THF/DMSO-90	...	1883 ± 814	570–4100
60	DCM/DMF-60	17 kV, 1 mL/h, 23 cm	1020 ± 276	560–2000
70	DCM/DMF-70	...	890 ± 172	550–1590
80	DCM/DMF-80	...	764 ± 135	430–1100
90	DCM/DMF-90	...	697 ± 141	450–1400
60	DCM/DMSO-60	12.5 kV, 1 mL/h, 23 cm	785 ± 163	480–1270
70	DCM/DMSO-70	...	1017 ± 265	630–2000
80	DCM/DMSO-80	...	980 ± 237	600–1700
90	DCM/DMSO-90	...	894 ± 193	500–1800
60	CF/DMF-60	17 kV, 1 mL/h, 23 cm	918 ± 423	360–2310
70	CF/DMF-70	...	1250 ± 554	440–2730
80	CF/DMF-80	...	879 ± 217	480–1700
90	CF/DMF-90	...	756 ± 256	300–1490
60	CF/DMSO-60	17 kV, 1 mL/h, 23 cm	582 ± 161	300–1340
70	CF/DMSO-70	...	586 ± 219	250–1400
80	CF/DMSO-80	...	745 ± 354	290–1500
90	CF/DMSO-90	...	870 ± 300	350–1500

80% [Fig. 3(d)] and surface features reached a maximum distribution level at 90% RH [Fig. 3(e)] in all DCM/DMF-based samples. However, the fiber surfaces exhibited almost smooth topography in the presence of rh [Fig. 3(a)]. PCL fibers from DCM/DMSO solutions had a highly porous structure beginning from 60% RH [Figs. 3(g)–3(j)]. Both breath figures and pores draw attention. The limited surface texture with a number of nanoindentations appeared on the control group [Fig. 3(f)]. When considering PCL fibers from the solvent system of CF/DMF, the control surfaces showed rough and indented morphology [Fig. 4(a)]. However, the surface texture of the fibers changed apparently depending on varying RH.

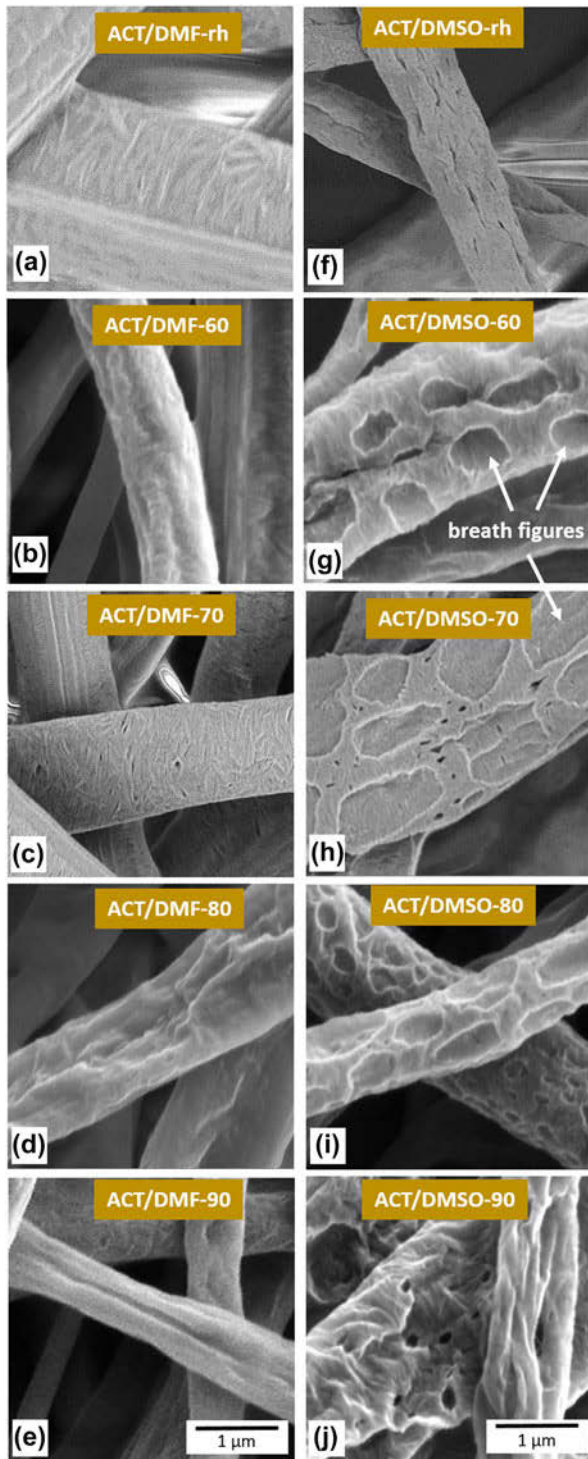


Figure 1: SEM images of PCL fibers from ACT/DMF and ACT/DMSO solvent/nonsolvent systems at different RH. (a, f) Room humidity, (b, g) 60%, (c, h) 70%, (d, i) 80%, and (e, j) 90%.

60% RH and 80% RH led to wrinkled surface texture, including a small number of pores for CF/DMF-60 [Fig. 4(b)] and CF/DMF-80 [Fig. 4(d)] samples, respectively, that was similar to DCM/DMF-60 and DCM/DMF-70 samples [Figs. 3(b) and

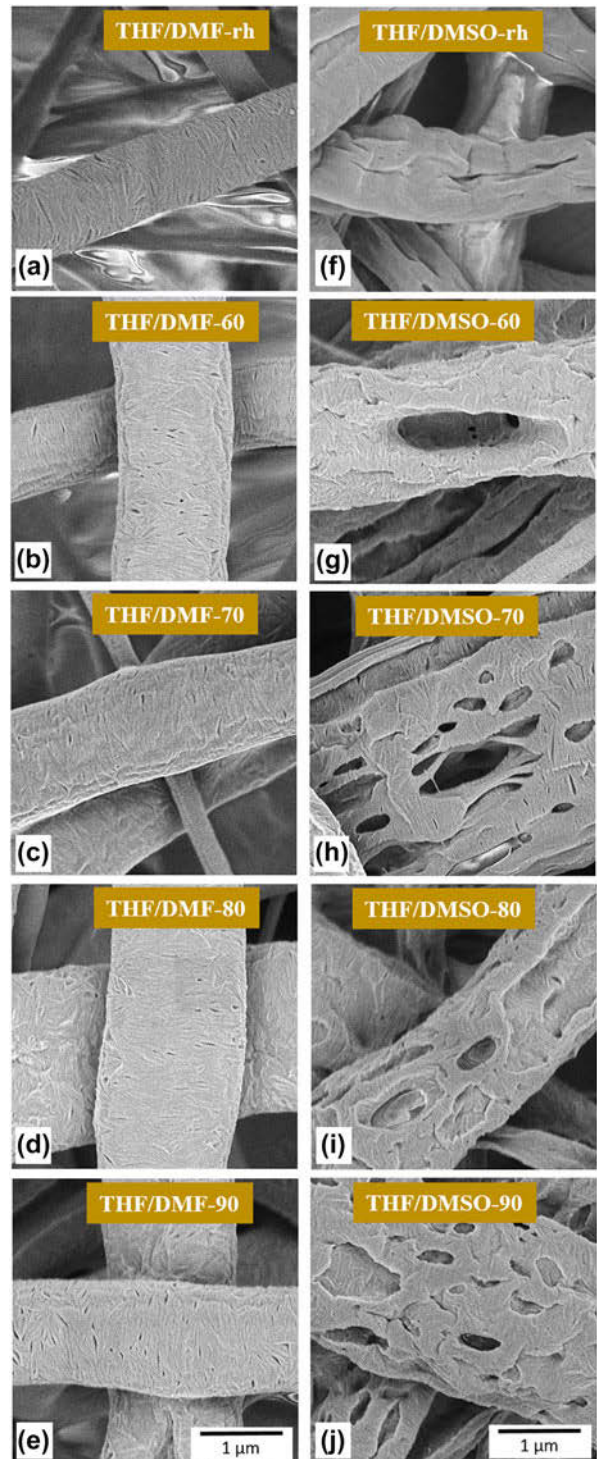


Figure 2: SEM images of PCL fibers from THF/DMF and THF/DMSO solvent/nonsolvent systems at different RH. (a, f) Room humidity, (b, g) 60%, (c, h) 70%, (d, i) 80%, and (e, j) 90%.

3(c)]. On the other hand, the fibers from CF/DMF-70 [Fig. 4(c)] and CF/DMF-90 [Fig. 4(e)] samples had better surface morphology in terms of porosity. It was clear that all individual PCL fiber surfaces covered better-arranged pores in

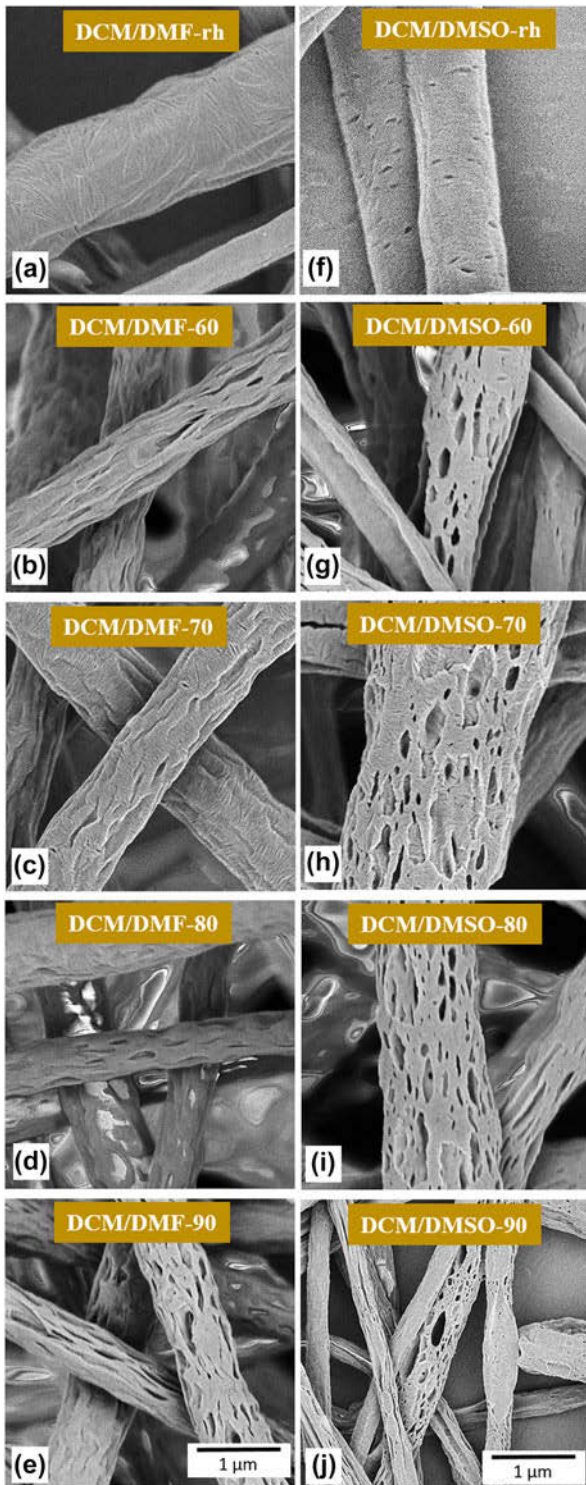


Figure 3: SEM images of PCL fibers from DCM/DMF and DCM/DMSO solvent/nonsolvent systems at different RH. (a, f) Room humidity, (b, g) 60%, (c, h) 70%, (d, i) 80%, and (e, j) 90%.

CF/DMF-90. Figures 4(f)–4(j) show the porous surface topography for CF/DMSO-based PCL solutions. CF/DMSO-70, CF/DMSO-80, and CF/DMSO-90 possessed different types of porous structures with a wide distribution of pore sizes.

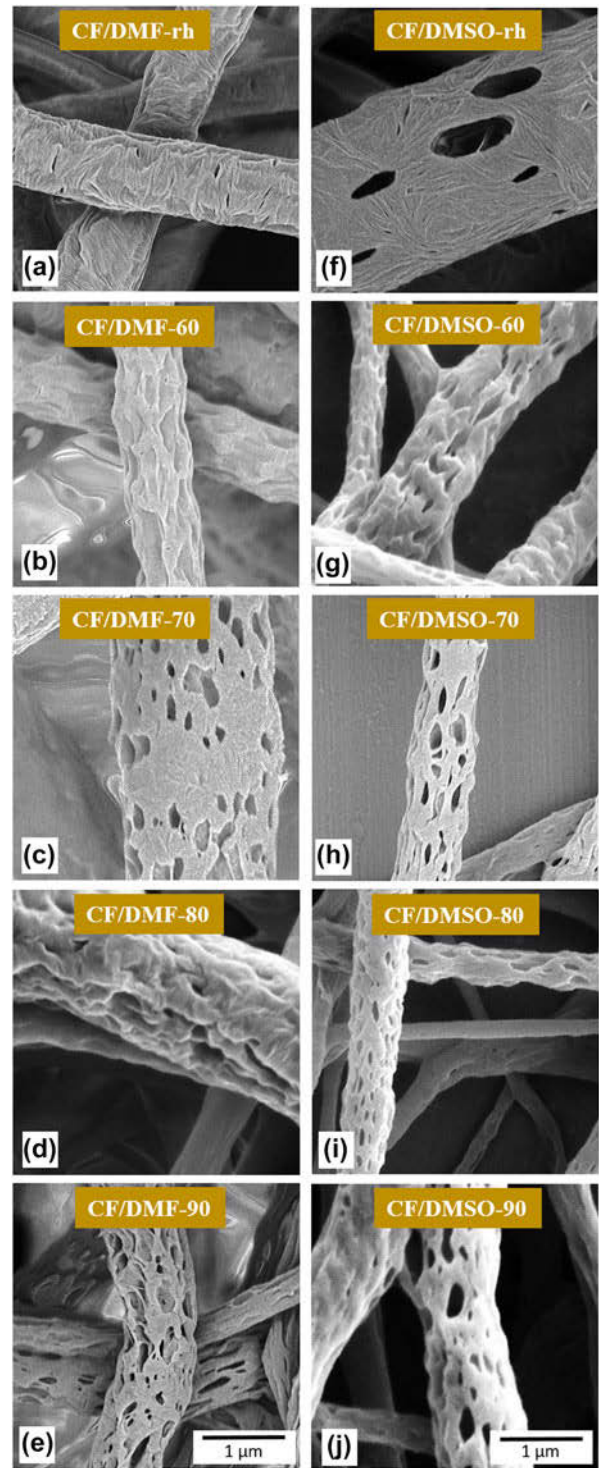


Figure 4: SEM images of PCL fibers from CF/DMF and CF/DMSO solvent/nonsolvent systems at different RH. (a, f) Room humidity, (b, g) 60%, (c, h) 70%, (d, i) 80%, and (e, j) 90%.

Figure 4(f) also indicated the successful formation of interconnected pores on the control group. Figure 5 shows atomic force microscope (AFM) images of ACT/DMSO-70 and CF/DMF-60 surfaces. The altered topography of the surfaces

revealed the effect of RH. The depth of breath figures on the fiber surfaces varied in the range of 20–150 nm. Table III presents Brunauer–Emmett–Teller (BET) surface areas, water contact angles, apparent porosities, and mechanical properties of the selected samples. Depending on various topographical textures on the fiber surfaces, the given surfaces had different surface areas. CF/DMF-60 had a maximum surface area, whereas CF/DMSO-80 had a minimum value. It would be possible to expect a high specific surface area because the surface roughness of CF/DMF-60 increased because of its wrinkled structure. The relatively lower surface area of the fibers from CF/DMSO-80 could be attributed to the fact that some fibers were highly porous, whereas the others had limited porosity [Fig. 4(i)]. We concluded that all areas of the fibrous mat exhibited similar structure, and this explained relatively less surface area for them. The surfaces exhibited a highly hydrophobic behavior as expected. However, a shift of the contact angle to 116° could be attributed to wider pores that absorbed the water drops a little for THF/DMSO-80. Apparent porosities of the samples, except for CF/DMSO-80, tended to increase depending on the increasing porosity. To elucidate how the mechanical properties of the fibers were affected by different morphologies, a stress–strain test was applied to the samples. Depending on different kinds of defects (Table III), the samples exhibited varying mechanical properties. CF/DMF-60 with a wrinkled structure had the highest tensile strength and strain% at break. On the other hand, the porous fibers showed a lower tensile strength and strain%. It was obvious that the presence of pores made the fibers mechanically weaker. As the strain increases, fibers elongate in the tensile direction. Simultaneously, pores are stretched parallel to the fiber axis. The fiber deformation occurs when the strain reaches a certain critical value. This deformation is facilitated by increasing porosity. Not only the presence of pores but also the depth of the pores led to the mechanically weaker fiber as observed in THF/DMSO-80 and CF/DMSO-80 samples. It was concluded that the flexibility of the fibers was restricted by these pores.

NIPS generally includes a cast polymer solution which is immersed in a nonsolvent bath to initiate phase separation [7, 26]. For the electrospinning technique, a solvent and a nonsolvent with an appropriate amount that does not cause phase separation before electrospinning can be mixed. During the subsequent solidification process, the composition changes and falls into the phase separation region because of the different volatility between solvent and nonsolvent, and thereby porous structures can be created [7, 27]. In the presented study, the morphological alterations observed in PCL fibers occurred through different routes depending on the solvent/nonsolvent system used under room humidity. It was obvious that the phase separation by NIPS became more dominant for the nonsolvent DMSO including system, especially for the fibers

from CF/DMSO. Georgiadou et al. [7] investigated the surface morphology of electrospun PCL fibers produced from various solvent systems (CF/DMSO, DCM/DMSO, THF/DMSO, and formic acid/DMSO at various ratios) under 30–40% RH. According to their results, the addition of a small amount of DMSO (10 and 20% v/v) led to a porous surface. In the case where THF/DMSO (80/20) was used, beads appeared on the produced fibers, which is inconsistent with our findings (Fig. 2). In a highly humid environment, water vapor acts as a nonsolvent, leading to VIPS, and also triggers the breath figure mechanism. Figure 6 illustrates a possible breath figure mechanism that surface textures were generated by water droplets assembled on the surface. The resulting pores were not typically uniform, and this may be attributed to the dynamic condition of the electrospinning jet as compared with the static conditions where the effect of breath figures was dominant in thin films [28]. The VIPS process typically occurs in the presence of high humidity ($>50\%$) [29]. In this process, a hydrophobic polymer, a high volatility solvent, and a water-miscible solvent are essential to encourage VIPS. Over the course of electrospinning, the water vapor in the atmosphere is absorbed into the polymer jet traveling to the collector. When water is introduced, polymer-rich and polymer-poor regions within the jet are created by the phase separation because the hydrophobic polymer accumulates out of the solution. Finally, surface pores along with electrospun fibers are obtained because the rapid evaporation of the highly volatile solvent locks in the phase-separated geometry. The pores created by VIPS are typically irregularly shaped [21, 29, 30]. To understand how the mechanism of phase separation affects the surface morphology of PCL fibers, the experimental studies were designed with four different solvents and two different nonsolvents in the presence or absence of high RH. Solvent miscibility with water was another factor to be taken into account for further understanding its effect (Table I). Contrary to previous publications [21, 29, 30], VIPS failed to induce pore formation when looking at the fiber surfaces from the solutions of ACT/DMF [Figs. 1(b)–1(e)] and THF/DMF [Figs. 2(b)–2(e)]. A possible explanation for that is hidden in their miscibility with water in the humid environment. It was hypothesized that the insufficient surface texture could be a result of the high absorption of water molecules which did not permit the rapid evaporation of both solvents to lock in the phase-separated geometry. The fiber formation process during electrospinning is based on solvent evaporation from the jet which travels to the collector. During the jet stretching, the DMF ratio increased gradually in the composition, whereas the high volatility solvent ratio reduces. Thus, DMF became a dominant factor to arise phase separation. However, because ACT and THF are miscible with water, the evaporation of both solvents from the jet was hindered because of the higher vapor

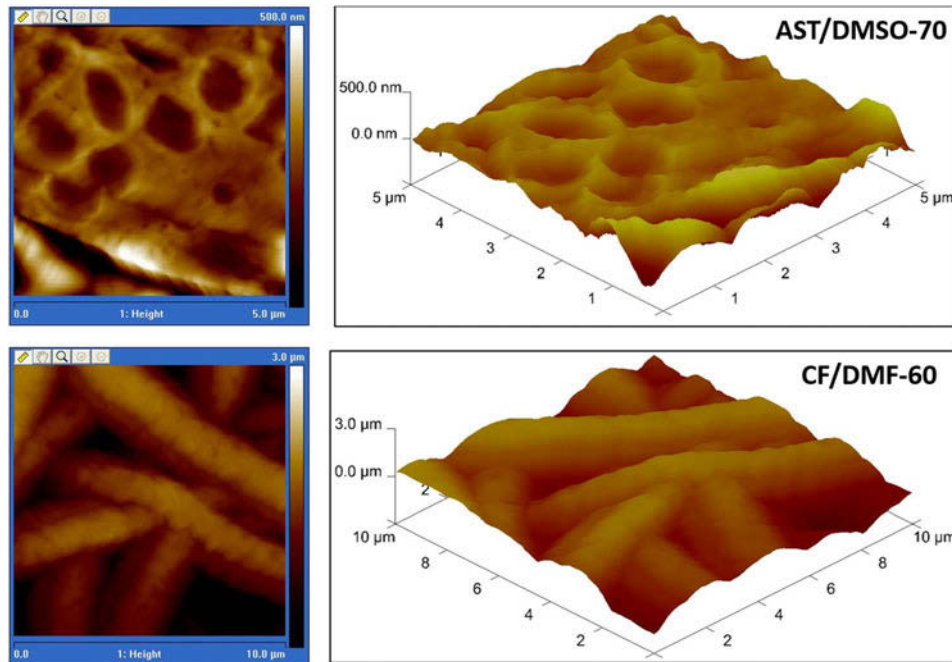


Figure 5: AFM images of ACT/DMSO-70 and CF/DMF-60.

TABLE III: Physical and mechanical properties of selected samples.

Samples	Type of texture	BET surface area (m ² /g)	Water contact angle (°)	Apparent porosity (%)	Breaking strain (%)	Tensile strength (MPa)
CF/DMF-60	Wrinkled	9.711 ± 1.669	130	76	379	5.69
ACT/DMSO-80	Breath figures	7.602 ± 0.970	122	78	261	5.72
THF/DMSO-80	Pores and breath figures	5.794 ± 0.917	116	81	210	5.26
CF/DMSO-80	Pores	2.347 ± 0.028	127	91	209	4.37

pressure of water absorbed. In addition to that, this miscibility allowed water to penetrate its molecules from shell to core of fiber jet, and thus thermodynamic instability leading to phase separation process was restricted to favor minimal defects on the fibers. Another explanation for that relates to the lower boiling point of DMF in contrast with DMSO. There is a race between solid skin formation and phase separation processes during the electrospinning process. This means that if the solidification is faster than phase separation, a relatively smooth topography appears. Otherwise, different surface properties occur. The diffusive solvent evaporation from both PCL solutions of ACT/DMF and THF/DMF occurred in less time when compared with those prepared with DMSO, which increased the evaporation time. Thus, this led to less time for thermodynamic instabilities. Topographical differences in the DMF- and DMSO-based fibers also supported this phenomenon that NIPS was much more dominated in all DMSO-based control groups. When high water vapor involves the spinning environment, then VIPS becomes a driving force for the phase separation. Besides, the higher density, viscosity, and surface

tension of the DMSO [31] might have contributed to defect formation. Similar to that, Megelski et al. [30] reported the surface roughness or microtexture of electrospun polystyrene (PS) fibers decreased as the ratio of less volatile DMF in THF/DMF solvent mixtures increased. Cosgriff-Hernandez et al. [29] reported that broken fibers below 50% RH were obtained from PCL solution with CF/DMF (80/20 v/v). Contrary to their findings, continuous fibers were obtained in the presented study [Fig. 4(a)]. One might be assumed that various factors (such as flow rate, applied voltage, and viscosity) involved in the formation of fibers at various morphologies during electrospinning. Lu and Xia [32] presented a simple and reliable method for generating PS yarns which had either internal porosity or surface roughness by using a proper combination of solvent and RH. They discovered that the low vapor pressure of DMF was critical for the evolution of pores in the interiors, whereas the relatively high vapor pressure of THF excelled in creating a rough surface. However, their combining of THF/DMF at a volume ratio of 50/50 had a very limited effect on the surface topography even for the highest RH (62%), which was

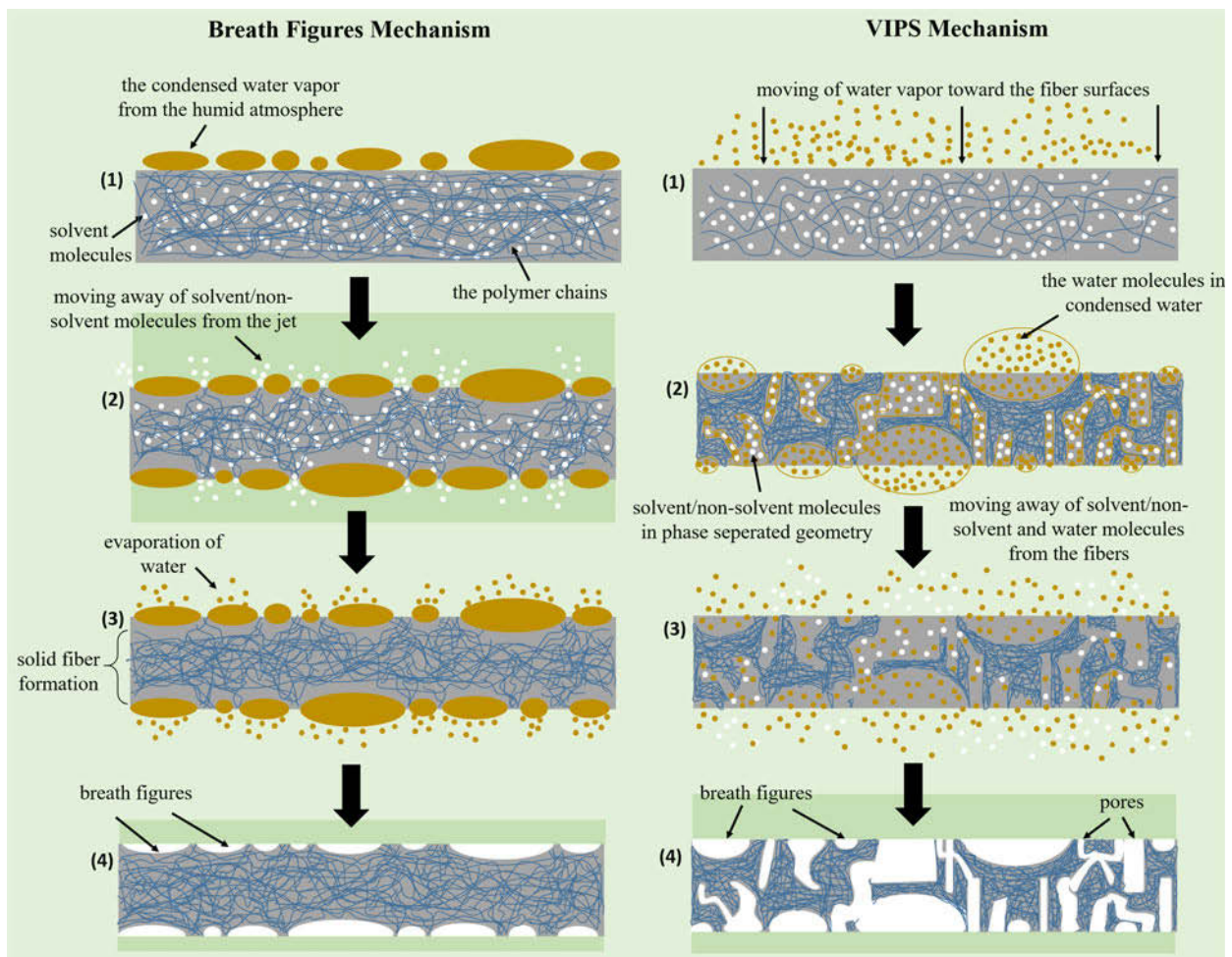


Figure 6: Estimated phase separation mechanisms induced by breath figures (left side) as follows: (1) water from humid atmosphere condenses on the jet. (2) Solvent evaporates through the condensed water droplets, the polymer chains inside the jet are arranged by moving away from water, and skin formation occurs. (3) Water molecules begin to move away from the surface of the jet by evaporation, leaving imprints. (4) Finally, breath figures appear on the fiber surface, and by VIPS (right side) as follows: (1) water from the humid atmosphere condenses on the jet (this can also initiate the abovementioned breath figure mechanism). (2) The initiation of the phase separation by the nonsolvent results in the organization of the polymer chains by generating polymer-poor cavities. Then, the cavities are occupied with water molecules that penetrate the jet and solvent/nonsolvent molecules at different ratios. (3) Solvent/nonsolvent and water molecules quit from the jet by leaving defects on the surface and inside of the as-spun fibers. (4) At the final step, the porous fibers at different characteristics are obtained after residual solvent/nonsolvent and water evaporate.

consistent with our observations (Figs. 1 and 2). In a study by Ding and coworkers [33], the THF/DMF mixing ratio in PS solutions was proved to be the key parameter to affect porous structure which was obtained because of the rapid evaporation of THF during electrospinning. According to their results, as the vapor pressure of the solvent mixtures decreased, the wrinkled or smooth surfaces were obtained as observed in our results. According to an early study by Rabolt et al. [30], if the vapor phase is saturated with solvent, skin formation can be hindered, which is possible for high volatile solvents. In this case, pore formation is determined by the vapor pressure of the nonsolvent and polymer concentration. Increasing RH or decreasing polymer concentration would increase the pore formation.

In the presented study, morphological changes observed on DCM- and CF-based samples conspicuously exhibited that both the NIPS and VIPS processes had an effect to alter the surface texture of PCL fibers. VIPS seemed to be the governing parameter to affect the surface morphology of the produced fibers. The estimated mechanism of VIPS is represented in Fig. 6. Contrary to the mechanism aforementioned, because DCM and CF are immiscible with water, the condensed water vapor from atmosphere accumulated to the jet surface, and this led to heterogenic solvent/nonsolvent phase separation in the liquid phase. As the solvents evaporated, the fraction of DMF or DMSO in solutions increased with time. Thus, the solution followed to phase separate into polymer-rich and solvent-rich phases. Besides, as a nonsolvent, the incorporation of water

from the humid environment to water-miscible DMF or DMSO lowered the solvent quality, which in turn accelerated the phase separation process. During the production of solid fiber surfaces, hydrophobic PCL chains precipitated toward to the higher volatile solvent phase. Meanwhile, the nonsolvents and the water molecules occupied the cavities in the polymer-poor phase formed as a result of the NIPS mechanism, and this process led to the porous structure (Figs. 3 and 4). The different types of surface morphology observed on the samples can be attributed to the phase separation mechanisms that followed various routes and the dynamic motion of spinning jet (stretching and whipping) affected by different solvent properties. Fortunato et al. [22] confirmed that irregular and interconnected surface topographies were obtained on PCL fibers by using the CF/DMSO solvent system in the presence of 35% RH or above. Similar results were obtained by Kotaki et al. [15], where electrospun PLA fibers were fabricated by using DCM/DMF 80/20 v/v in the presence of 80% RH.

It is worth to mention that solvent evaporation as an endothermic process removes heat from the solution and therefore causes a temperature decrease on the jet surface because of the latent heat loss to a minimum temperature [the wet-bulb temperature (T_{wb})]. Besides, the temperature to which air can be cooled down reaching full saturation is the dew point (T_{dp}). The extent of this decrease depends on the volatility of solvents. When saturated air encounters a surface colder than its temperature (in this case $T_{dp} > T_{wb}$), water condensation is triggered [22]. This results in changing the smooth fiber structure to defected topography. The difference between these two temperatures determined the degree of water condensation on fiber surfaces and further altering of the fiber surface. The higher the solvent volatility, the lower the T_{wb} . Additionally, rising environmental RH increased T_{dp} .

It can be suggested that ACT/DMSO-60, CF/DMF-60, and CF/DMSO-70 may be preferable for PCL fibers with breath figures, and wrinkled or porous structure, respectively.

Conclusion

Various topographical structures, especially pores, on the outer and inner structures of nanofibers reveal an emergent class of nanoporous materials with a maximum specific surface area, high pore volume, and extreme adsorption capacity that could lead to improvement in many applications such as tissue engineering, medical applications, catalysts, sensors, batteries, energy storage, adsorption/separation, and filtration. Clarifying the effect of surface topography on cellular behavior is essential to achieve both the fundamental understanding of complex cell-material interactions and advancements in biomaterials applications. Further researches are still needed to obtain of various kinds of surface defects on a variety of polymeric nanofibers.

In the presented study, the production of PCL fibers at various topographic details was achieved through a single-step process from a variety of solvent/nonsolvent systems in the presence of different RH conditions. The type of solvent and nonsolvent and the degree of RH determined the surface property of the fibers. In addition to that, solvent miscibility with water was another important factor that affected the surface topography. Thus, CF- and DCM-based solutions were much more effective, whereas DMSO had a higher impact on ACT- and THF-based solutions depending on RH. It was concluded that breath figures, VIPS, and NIPS mechanisms contributed in various ratios to convert smooth surfaces to defected ones. Overall, the fiber surfaces exhibited porous, eroded, wrinkled, or/and rough topography. In our ongoing studies, we will focus on cellular responses to the different kinds of surfaces obtained here to reveal the best surfaces in terms of cell-biomaterial interaction.

Materials and methods

PCL (average $M_n = 80,000$ Dalton) was purchased from Sigma-Aldrich. CF (99.0%, ACS reagent grade), DMSO (99.9%), and DMF (99.5%, ACS reagent grade) were purchased from Merck, Germany. ACT (99.5%), DCM (99.8%, stabilized with amylene), and THF (99.0%, stabilized with butylated hydroxytoluene) were ACS reagent grade and purchased from Sigma-Aldrich, USA.

A closed-system electrospinning device (NSE-300, Invenso Ltd., Turkey) was used for experiments. A solvent (80 mL per 100 mL) and a nonsolvent (20 mL per 100 mL) were added to a bottle including PCL granules (11 g per 100 mL), respectively. Then, the mixtures were magnetically stirred overnight in room conditions to dissolve the polymer completely. The electrospinning of PCL solutions was conducted at room temperature (18–22 °C) under various RH (60–90%). PCL fibers were collected on an aluminum foil fixed onto the stationary collector. The fiber samples were dried at room temperature for at least three days to remove residual solvents and then kept in a desiccator for further use. The tip of the needle to collector distance was set up at 23 cm for all experiments. Detailed electrospinning conditions are given in Table II.

The surface of PCL fibers was analyzed by SEM (GAIA 3, Tescan Corporation, Czech Republic) and AFM (Multimode V, Veeco Instruments Inc., USA) operating at tapping mode. Before SEM analysis, fiber samples were sputtered with gold-palladium. Fiber diameters and pore sizes were calculated by ImageJ program (National Institutes of Health, USA). The water contact angles of electrospun fiber mats were measured by Drop Shape Analyzer (DSA100, Germany) at room temperature immediately after the deionized water droplet made contact with the fiber surface. BET surface areas were

determined from N₂ adsorption isotherm data collected at 77 K (TRISTAR II, Micromeritics, USA). Before analysis, fibers were degassed for at least 6 h at 20 °C. Mechanical properties were observed by a texture analysis instrument (TA.XTplusC, Stable Micro Systems Ltd., UK). PCL fibrous matrix were cut in small sizes and their thickness, length, width, and weight were measured. The determined values were substituted in Eq. (1) to calculate the apparent density. Then, the determined apparent density and standard density (bulk density) of PCL were substituted in Eq. (2) to measure the average porosity percentage.

$$\text{Matrix apparent density (g/cm}^3\text{)} = \frac{\text{mass of matrix (g)}}{\text{matrix thickness (cm)} \times \text{matrix area (cm}^2\text{)}} \quad (1)$$

$$\text{Matrix porosity (\%)} = \left(1 - \frac{\text{matrix apparent density (g/cm}^3\text{)}}{\text{bulk density (g/cm}^3\text{)}}\right) \times 100 \quad (2)$$

Acknowledgments

This study was supported by İnönü University Scientific Researches Project unit under the project number of FBA-2018-1332. I would like to thank Professor Menemşe GÜMÜŞDERELİOĞLU, Ph.D. researcher Zeynep ALTINIŞIK, and Assistant Professor Cem BAYRAM for their valuable supports in this study.

References

1. Z.-M. Huang, Y.Z. Zhang, M. Kotaki, and S. Ramakrishna: A review on polymer nanofibers by electrospinning and their applications in nanocomposites. *Compos. Sci. Technol.* **63**, 2223 (2003).
2. S.Y. Chew, Y. Wen, Y. Dzenis, and K.W. Leong: The role of electrospinning in the emerging field of nanomedicine. *Curr. Pharm. Des.* **12**, 4751 (2006).
3. S.G. Kumbar, R. James, S.P. Nukavarapu, and C.T. Laurencin: Electrospun nanofiber scaffolds: Engineering soft tissues. *Biomed. Mater.* **3**, 034002 (2008).
4. T.J. Sill and H.A. von Recum: Electrospinning: Applications in drug delivery and tissue engineering. *Biomaterials* **29**, 1989 (2008).
5. B. Azimi, P. Nourpanah, M. Rabiee, and S. Arbab: Poly(ϵ -caprolactone) fiber: An overview. *J. Eng. Fibers Fabr.* **9**, 155892501400900309 (2014).
6. J. Zhang, T. Zheng, E. Alarçin, B. Byambaa, X. Guan, J. Ding, Y.S. Zhang, and Z. Li: Porous electrospun fibers with self-sealing functionality: An enabling strategy for trapping. *Biomacromolecules* **13**, 1701949 (2017).
7. K.A.G. Katsogiannis, G.T. Vladislavljević, and S. Georgiadou: Porous electrospun polycaprolactone (PCL) fibres by phase separation. *Eur. Polym. J.* **69**, 284 (2015).
8. A. Senthamizhan, B. Balusamy, A. Celebioglu, and T. Uyar: "Nanotraps" in porous electrospun fibers for effective removal of lead(II) in water. *J. Mater. Chem. A* **4**, 2484 (2016).
9. A. Soundararajan, J. Muralidhar R., R. Dhandapani, J. Radhakrishnan, A. Manigandan, S. Kalyanasundaram, S. Sethuraman, and A. Subramanian: Surface topography of polylactic acid nanofibrous mats: Influence on blood compatibility. *J. Mater. Sci.: Mater. Med.* **29**, 145 (2018).
10. Y. Wang, J. Deng, R. Fan, A. Tong, X. Zhang, L. Zhou, Y. Zheng, J. Xu, and G. Guo: Novel nanoscale topography on poly(propylene carbonate)/poly(ϵ -caprolactone) electrospun nanofibers modifies osteogenic capacity of ADCs. *RSC Adv.* **5**, 82834 (2015).
11. Y. Hu, S.R. Winn, I. Krajbich, and J.O. Hollinger: Porous polymer scaffolds surface-modified with arginine-glycine-aspartic acid enhance bone cell attachment and differentiation in vitro. *J. Biomed. Mater. Res., Part A* **64**, 583 (2003).
12. L. Moroni, R. Licht, J. de Boer, J.R. de Wijn, and C.A. van Blitterswijk: Fiber diameter and texture of electrospun PEOT/PBT scaffolds influence human mesenchymal stem cell proliferation and morphology, and the release of incorporated compounds. *Biomaterials* **27**, 4911 (2006).
13. G.-M. Kim, R. Lach, G.H. Michler, and Y.-W. Chang: The mechanical deformation process of electrospun polymer nanocomposite fibers. *Macromol. Rapid Commun.* **26**, 728 (2005).
14. C.L. Casper, J.S. Stephens, N.G. Tassi, D.B. Chase, and J.F. Rabolt: Controlling surface morphology of electrospun polystyrene fibers: Effect of humidity and molecular weight in the electrospinning process. *Macromolecules* **37**, 573 (2004).
15. Y. Li, C.T. Lim, and M. Kotaki: Study on structural and mechanical properties of porous PLA nanofibers electrospun by channel-based electrospinning system. *Polymer* **56**, 572 (2015).
16. K.A.G. Katsogiannis, G.T. Vladislavljević, and S. Georgiadou: Porous electrospun polycaprolactone fibers: Effect of process parameters. *J. Polym. Sci., Part B: Polym. Phys.* **54**, 1878 (2016).
17. L. Zhang and Y.-L. Hsieh: Nanoporous ultrahigh specific surface polyacrylonitrile fibres. *Nanotechnology* **17**, 4416 (2006).
18. H.R. Pant, M.P. Neupane, B. Pant, G. Panthi, H.-J. Oh, M.H. Lee, and H.Y. Kim: Fabrication of highly porous poly(ϵ -caprolactone) fibers for novel tissue scaffold via water-bath electrospinning. *Colloids Surf., B* **88**, 587 (2011).
19. M. Srinivasarao, D. Collings, A. Philips, and S. Patel: Three-dimensionally ordered array of air bubbles in a polymer film. *Science* **292**, 79 (2001).
20. T.H. Nguyen, T.Q. Bao, I. Park, and B.T. Lee: A novel fibrous scaffold composed of electrospun porous poly(ϵ -caprolactone) fibers for bone tissue engineering. *J. Biomater. Appl.* **28**, 514 (2013).
21. E.S. Medeiros, L.H.C. Mattoso, R.D. Offeman, D.F. Wood, and W.J. Orts: Effect of relative humidity on the morphology of electrospun polymer fibers. *Can. J. Chem.* **86**, 590 (2008).
22. G. Yazgan, R.I. Dmitriev, V. Tyagi, J. Jenkins, G.-M. Rotaru, M. Rottmar, R.M. Rossi, C. Toncelli, D.B. Papkovsky,

- K. Maniura-Weber, and G. Fortunato:** Steering surface topographies of electrospun fibers: Understanding the mechanisms. *Sci. Rep.* **7**, 158 (2017).
23. **D. Lubasova and L. Martinova:** Controlled morphology of porous polyvinyl butyral nanofibers. *Journal of Nanomaterials* **2011**, 6 (2011).
24. **Z. Qi, H. Yu, Y. Chen, and M. Zhu:** Highly porous fibers prepared by electrospinning a ternary system of nonsolvent/solvent/poly(l-lactic acid). *Mater. Lett.* **63**, 415 (2009).
25. **A. Luwang Laiva, J.R. Venugopal, S. Sridhar, B. Rangarajan, B. Navaneethan, and S. Ramakrishna:** Novel and simple methodology to fabricate porous and buckled fibrous structures for biomedical applications. *Polymer* **55**, 5837 (2014).
26. **J.T. Jung, J.F. Kim, H.H. Wang, E. di Nicolo, E. Drioli, and Y.M. Lee:** Understanding the non-solvent induced phase separation (NIPS) effect during the fabrication of microporous PVDF membranes via thermally induced phase separation (TIPS). *J. Membr. Sci.* **514**, 250 (2016).
27. **P.-Y. Chen and S.-H. Tung:** One-step electrospinning to produce nonsolvent-induced macroporous fibers with ultrahigh oil adsorption capability. *Macromolecules* **50**, 2528 (2017).
28. **E. Bormashenko:** Breath-figure self-assembly, a versatile method of manufacturing membranes and porous structures: Physical, chemical and technological aspects. *Membranes* **7**, 45 (2017).
29. **R.M. Nezarati, M.B. Eifert, and E. Cosgriff-Hernandez:** Effects of humidity and solution viscosity on electrospun fiber morphology. *Tissue Eng., Part C* **19**, 810 (2013).
30. **S. Megelski, J.S. Stephens, D.B. Chase, and J.F. Rabolt:** Micro- and nanostructured surface morphology on electrospun polymer fibers. *Macromolecules* **35**, 8456 (2002).
31. **N. Ucar, N. Kizildag, A. Onen, I. Karacan, and O.J.F. Eren:** Polymers: Polyacrylonitrile-polyaniline composite nanofiber webs: Effects of solvents, redoping process and dispersion technique. *Fibers Polym.* **16**, 2223 (2015).
32. **P. Lu and Y. Xia:** Maneuvering the internal porosity and surface morphology of electrospun polystyrene yarns by controlling the solvent and relative humidity. *Langmuir* **29**, 7070 (2013).
33. **J. Lin, B. Ding, J. Yu, and Y. Hsieh:** Direct fabrication of highly nanoporous polystyrene fibers via electrospinning. *ACS Appl. Mater. Interfaces* **2**, 521 (2010).